Microwave heat-drawing of poly(oxymethylene): effect of molecular weight on drawing behaviour and mechanical properties

K. Nakagawa and T. Konaka
NTT Ibaraki Electrical Communication Laboratories, Nippon Telegraph and Telephone Corporation, Tokai, Ibaraki, 319-11, Japan
(Received 30 April 1985; revised 19 July 1985)

The drawing behaviour of a series of poly(oxymethylene) homopolymers with number-average molecular weight ($\bar{M}_n$) ranging from 38 000 to 66 000 has been studied at a feed speed of 0.06 m min^{-1} under microwave heating. Tubes with outer and inner diameter of 4 mm and 1 mm, respectively, were used for drawing experiments. The optimum tensile load and ambient temperature for high modulus increased with $\bar{M}_n$. The highest tensile modulus (54 GPa) and strength (1.6 GPa) were obtained for higher $\bar{M}_n$ samples, although the attainable draw ratio decreased from 34 to 28 with increase of $\bar{M}_n$.

(Keywords: poly(oxymethylene); molecular weight; drawing; microwave heating; mechanical properties)

INTRODUCTION

Recently we have shown that ultrahigh modulus poly(oxymethylene) (POM) with tensile modulus of ~60 GPa (draw ratio, λ, more than 30) can be produced by tensile drawing under microwave heating[1-5]. It is well known that the tensile drawing behaviour of polymers depends on molecular weight and its distribution[6]. The influence of molecular weight on the drawing behaviour of POM has been studied by conventional tensile testing[7]. It has been shown that the optimum grade for high draw and high modulus is Delrin 500 grade ($\bar{M}_n = 45\,000$). In the microwave heat-drawing method, however, the optimum molecular weight may be different from that in the conventional drawing method. In this paper we describe an investigation in which the influence of molecular weight on drawing behaviour under microwave heating and the resultant mechanical properties were examined.

EXPERIMENTAL

Samples

The materials used were four grades of the commercially available POM homopolymer, Tenac (Asahi Chemical Industry Co., Japan). The molecular weight characteristics of the different grades are given in *Table 1*. Tubes with outer and inner diameter of 4 mm and 1 mm, respectively, were prepared from pellets by extrusion and used for drawing experiments under microwave heating. The drawn tubes may be used for strength members of optical fibre cables, because they are self-standing unlike fibres or films.

Drawing apparatus

Figure 1 shows the apparatus for drawing under microwave heating. The apparatus comprises a feed reel (2), thickness gauges (3), a feeder (4), a three-point bend type tension meter (5), microwave heating furnaces (6), microwave power sources (7), a take-up machine (8), and a take-up reel (9). Unlike a previous apparatus, the microwave heating furnace was divided into two furnaces for which the microwave power was controlled independently. The front short furnace (0.5 m long) was used to make a neck point, while the rear long furnace (3 m long) was used for ultradrawing the sample.

Figure 2 shows the microwave circuits. Continuous wave magnetrons (frequency 2.45 GHz, maximum power 1.5 kW) were used as the microwave power sources (1). For the front furnace, a dummy load (10) was connected to the matching waveguide (8) in order to dissipate the excess of microwave power. The reflected power was minimized with a triple stub tuner (5). For the rear furnace, a rectangular tapered waveguide (2), a power monitor (4) and a reflecting plate (11) were connected in turn to the matching waveguide (8). The electric field strength in the microwave heating furnace (9) was enhanced by reflecting the transmitted microwave at the reflecting plate (11). The transmitted power was maximized with the triple stub tuner (5).

Figure 3 shows the structure of the microwave heating furnace. Although a circular waveguide was used for the furnace in our previous work, the furnace was altered to a rectangular waveguide in which comb type electrodes were attached at equal distances of 2 cm along the draw direction as seen in the Figure. This alteration decreased

Table 1 Molecular weight characteristics for POM samples

Sample	Melt flow index	$\bar{M}_n$
1	2.2	66 000
2	2.5	63 000
3	9.2	47 000
4	18.0	38 000

0032-3861/86/071037-07$03.00

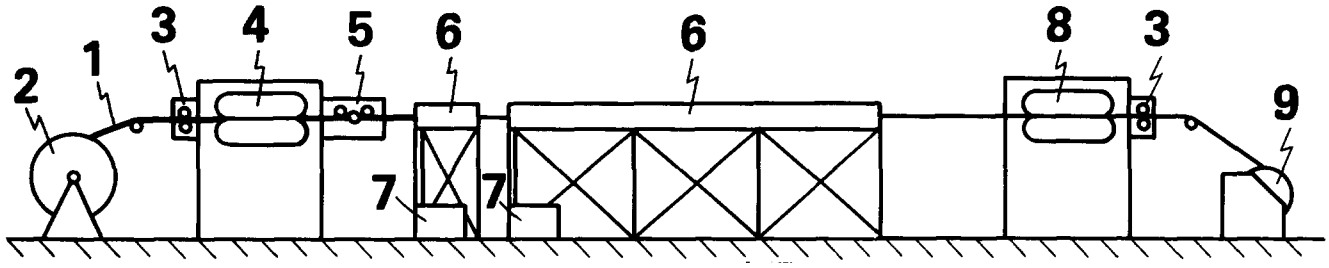

Figure 1 Microwave heating drawing apparatus. (1) sample; (2) feed reel; (3) thickness gauge; (4) feeder; (5) tension meter; (6) microwave heating furnace; (7) microwave power source; (8) take-up machine; (9) take-up reel

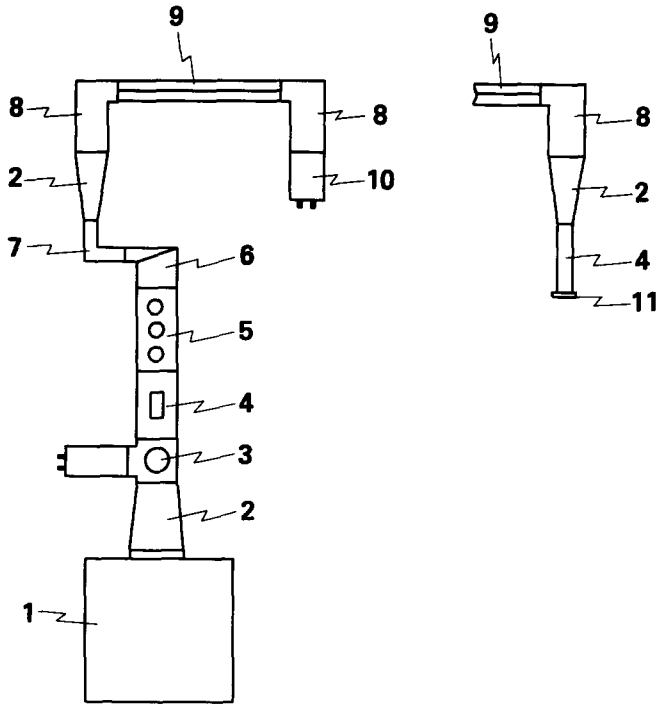

Figure 2 Schematic diagram of microwave circuit. (1) power source; (2) rectangular tapered waveguide; (3) isolator; (4) power monitor; (5) triple stub tuner; (6) H-bend; (7) E-bend; (8) rectangular waveguide for matching; (9) microwave heating furnace; (10) dummy load; (11) reflecting plate

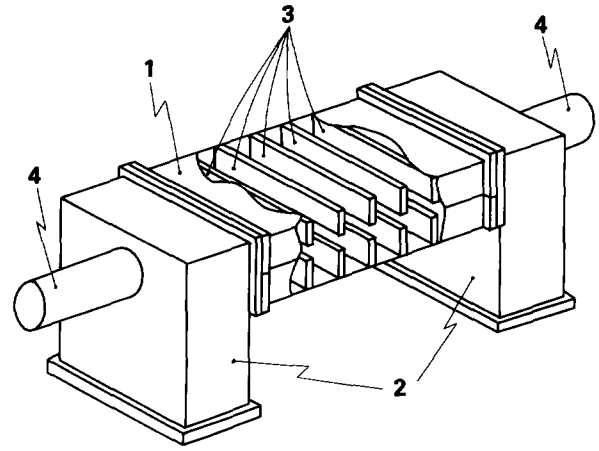

Figure 3 Structure of microwave heating furnace. (1) rectangular waveguide for heating; (2) rectangular waveguide for matching; (3) comb type electrodes; (4) sample gateway

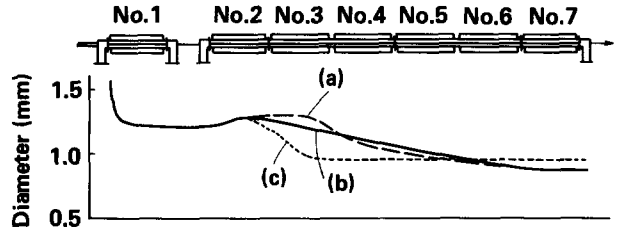

Figure 4 Drawing behaviour of sample 1 in furnaces. Feed speed 0.06 m min^{-1}; tensile load 21.$_5$ kg; ambient temperature: No. 1, 30°C; No. 2 (a) 110°C, (b) 120°C, (c) 140°C; No. 3 to No. 7, 130°C; maximum draw ratio: (a) 28, (b) 28, (c) 20; sonic modulus: (a) 44 GPa, (b) 48 GPa, (c) 36 GPa

the distance of standing wave in the furnace from 25 cm to 4 cm. The stepwise heating of the sample along the draw direction was depressed and the neck point was stabilized. A quartz glass tube with a diameter of ~2 cm was inserted in the rear furnace in order to facilitate setting up the sample.

Electric heaters were mounted around the rectangular waveguides in order to control the ambient temperature of the inside of the furnace. For the rear furnace the electric heaters were divided into six sections (No. 2 to No. 7) along the draw direction (as shown in *Figure 4*) and the temperature of each was controlled independently.

Drawing procedure

All drawing experiments were made at a constant feed speed of 0.06 m min^{-1}. The ambient temperature in the front furnace (No. 1) was kept at 30°C. The ambient temperatures in the sections (No. 2 to No. 7) of the rear furnace were kept at the desired temperatures in advance. After the sample had passed through the furnaces, the drawing was started at a given tensile load. The take-up speed was automatically controlled to hold the tensile load. Then the front furnace was operated at ~0.8 kW to make a neck point. After the undrawn sample was taken up from the rear furnace, the output of the rear furnace was gradually increased. With increasing the output the take-up speed increased to keep the tensile load constant. Finally the slenderized drawn sample was broken in the furnace at a specific output. Sonic modulus measurements were immediately made for the drawn sample obtained at a steady state just before it was broken. Such drawing experiments were made at various ambient temperatures of the rear furnace and tensile loads in order to find optimum conditions for each sample.

Mechanical measurements

Sonic moduli (E_s) of drawn samples were measured at room temperature with a direct reading pulse propagation viscoelastometer (DDV-5-B, Toyo Baldwin Co., Japan). The value of E_s was calculated from the following equation:

$$E_s = (L/t)^2 \rho \quad (1)$$

where L is the pulse propagation length (40 cm), t is the propagation time, and ρ is the sample density. For all

drawn samples a constant value of 1.42 g cm^{-3} was used for ρ. The pulse frequency was 10 kHz.

Dynamic mechanical measurements were performed at 3.5 Hz on samples 7 cm long with a Rheovibron DDV-3-EA (Toyo Baldwin Co., Japan). Tensile strength and elongation at break were measured at room temperature on a tensile testing machine. The experimental details have been published previously[4] and in the preceding paper[8].

Void fraction measurements

The volume fraction of internal voids (f_v) was calculated from the following equation[9]

$$f_v = 1 - \rho_{app}/\rho \quad (2)$$

where ρ_{app} is the apparent macroscopic density determined by weighing and measuring the dimensions of samples, and ρ is the density measured by the gradient column method. Since the ρ values were in the range 1.41 to 1.43 g cm^{-3} regardless of the draw ratio, as shown in *Figure 5*, a constant value of 1.42 g cm^{-3} was used for ρ[4]. If the gradient column fluid does not fully penetrate the voids within the ultradrawn samples, the ρ values are underestimated. But the real fraction of the internal voids cannot be lower than that estimated by equation (2).

Differential scanning calorimetry

The melting behaviour of drawn samples was examined using a Perkin–Elmer DSC-2. The measurements were made at a heating rate of 10 K min^{-1} on 5 mg samples. The temperature and the heat of fusion were calibrated with standard indium.

RESULTS AND DISCUSSION

Influence of ambient temperature gradient

Figure 4 shows the influence of ambient temperature gradient on the drawing behaviour of sample 1. The tensile load was fixed at 21.$_5$ kg. Almost all the ambient temperatures (No. 3 to No. 7) of the rear furnace were kept at the same temperature of 130°C. Only the ambient temperature (No. 2) near the inlet of the rear furnace was changed from 110°C (a) to 140°C (c). After the drawn sample was broken, the diameter in the furnaces was measured along the draw direction.

In the front furnace a neck point was made near the inlet of the front furnace and the sample was drawn up to $\lambda \sim 11$, which was calculated from the diameter of about 1.2 mm. The drawn sample was reheated in the rear

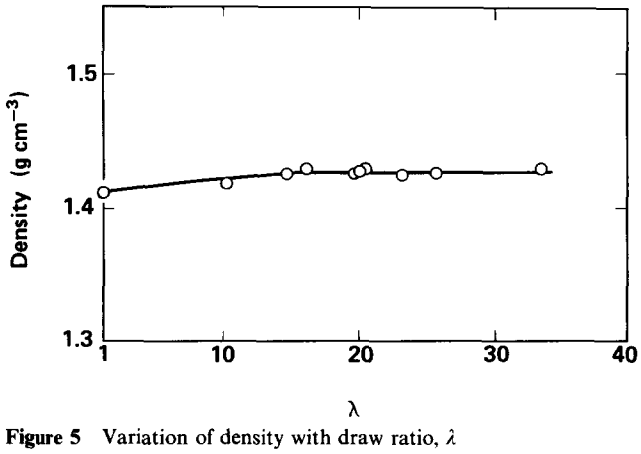

Figure 5 Variation of density with draw ratio, λ

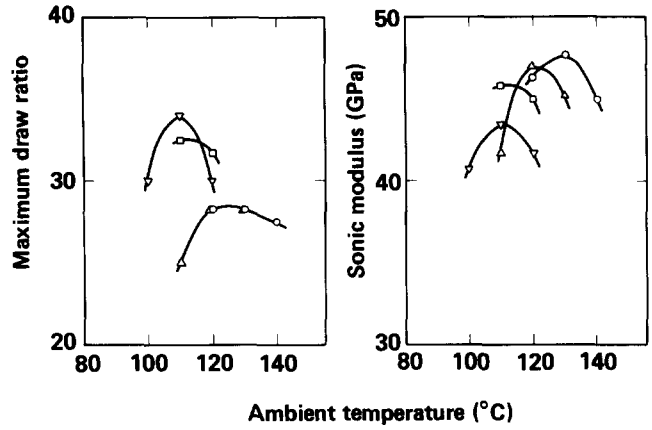

Figure 6 Variation of maximum draw ratio and sonic modulus with ambient temperature, ○, sample 1 (tensile load 21.$_5$ kg); △, sample 2 (19 kg); □, sample 3 (17 kg); ▽, sample 4 (16 kg)

furnace. The sample diameter increased near the inlet of the rear furnace by the thermal shrinkage and then decreased along the draw direction. The change of the diameter in the furnace was strongly affected by the ambient temperature (No. 2) near the inlet of the furnace. This resulted in a change of sonic modulus for the drawn sample. When the ambient temperature (No. 2) was 120°C, the highest sonic modulus of 48 GPa was obtained as given in *Figure 4(b)*. In this way it is necessary to set the ambient temperature gradient along the draw direction for high draw and high modulus. In all drawing experiments an attempt was made to make the ambient temperature gradient most suitable at a given tensile load and at a given ambient temperature of the rear furnace.

Influence of ambient temperature

Figure 6 shows the influence of ambient temperature on λ_{max} and attainable sonic modulus; λ_{max} in *Figures 6* and *7* refers to the ratio of maximum take-up speed to feed speed. The ambient temperature (axis or abscissas) refers to the ambient temperature near the outlet of the rear furnace. As mentioned above, the ambient temperatures of several sections at the inlet side of the rear furnace were adjusted at a given ambient temperature for high modulus; the tensile load was fixed at an optimum tensile load for each sample. There is an optimum ambient temperature for each sample, which increases with molecular weight.

Influence of tensile load

Although the sample temperature is specified in the conventional drawing method, it is difficult to measure the sample temperature in the furnace during microwave heating. Tensile load reflects the sample temperature, i.e. the tensile load increases with the decrease of the sample temperature at a given draw ratio. Accordingly, the tensile load was used as one of the parameters for drawing experiments. *Figure 7* shows the influence of tensile load on λ_{max} and attainable sonic modulus. There is an optimum tensile load for each sample. The optimum tensile load increases with the molecular weight. The optimum drawing conditions such as ambient temperature, ambient temperature gradient and tensile load were determined for each sample in this way.

Strain rate

Figure 8 shows the diameter changes in the furnaces under optimum conditions for samples 1 to 4. In the front

furnace a neck point is made and then the sample is ultradrawn in the rear furnace. The behaviour of the diameter change in the ultradrawing process depends on the sample. In sample 1 with the highest $\bar{M}_n$ the diameter gradually decreases over the whole rear furnace length, while the diameter of sample 4 with the lowest $\bar{M}_n$ rapidly decreases and only about 1 m length of the rear furnace is used to ultradraw the sample.

The strain rate γ is defined as follows,

$$\gamma = (dl/dt)/l \tag{3}$$

where l is the sample length and t is the time. Assuming the constant volume during the draw process, the sample diameter D is given by the following equation,

$$D = D_0 \exp(-\gamma t/2) \tag{4}$$

The sample speed v at a displacement x along the draw direction is expressed by:

$$v = v_0 \exp \gamma t \tag{5}$$

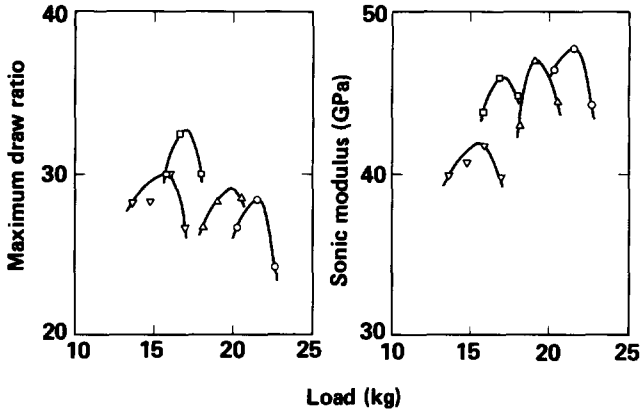

Figure 7 Variation of maximum draw ratio and sonic modulus with tensile load. ○, sample 1 (ambient temperature 130°C); △, sample 2 (120°C); □, sample 3 (110°C); ▽, sample 4 (120°C)

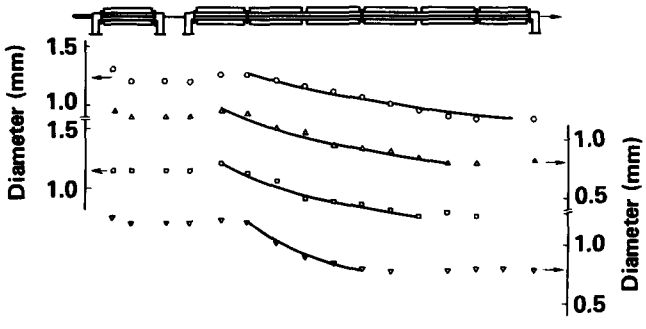

Figure 8 Diameter changes in furnaces under optimum conditions. ○, sample 1; △, sample 2; □, sample 3; ▽, sample 4; ———: calculated diameter change under constant strain rate

and

$$x = (v_0/\gamma)(\exp \gamma t - 1) \tag{6}$$

When the sample diameter decreases from D_0 to D_1 at a distance X, the diameter D at an arbitrary displacement x is given from these equations as follows,

$$D = D_0[(x/X)\{(D_0/D_1)^2 - 1\} + 1]^{-1/2} \tag{7}$$

The strain rate γ is calculated from the following equation,

$$\gamma = (V - v_0)/X \tag{8}$$

where V and v_0 are the speeds at $x = X$ and $x = 0$, respectively.

The curves in *Figure 8* represent the diameter changes calculated from equation (7). The observed diameter changes agree well, which means that the sample is drawn at a constant strain rate under the optimum drawing condition in the ultradrawing process and that the optimum strain rate depends on the sample. In equation (8) X is the distance in which the sample is slenderized in the rear furnace. For example, X is 2.5 m for sample 1, 1.0 m for sample 4. V is the final take-up speed and v_0 is the product of the feed speed (0.06 m min^{-1}) and the draw ratio, which is calculated from the diameter near the inlet of the rear furnace. The calculated values for γ are given in *Table 2*.

Optimum drawing conditions

Optimum drawing conditions for samples 1 to 4 are summarized in *Table 2*. High modulus materials can be produced for all the samples by microwave heat drawing under optimum conditions, although the attainable modulus is a little lower for sample 4, with the lowest $\bar{M}_n$. The optimum tensile load and ambient temperature for high modulus increase with $\bar{M}_n$, while the optimum strain rate (maximum draw ratio) decreases with $\bar{M}_n$. This may be due to high entanglements in samples of higher molecular weight.

In the conventional tensile drawing method the optimum grade for high draw and high modulus has been reported to be Delrin 500 grade ($\bar{M}_n = 45\,000$)[7], which corresponds to sample 3 in this work. In the microwave heating drawing method high modulus materials can be produced even for samples with much higher molecular weights.

In previous publications[1-3], the samples used were mistakenly reported to be POM homopolymer (Tenac 5010) with $\bar{M}_n = 37\,000$. The samples were in fact Delrin 100 grade ($\bar{M}_n = 66\,000$), corresponding to sample 1 in this work.

Table 2 Optimum drawing conditions under microwave heating

Sample	Load (kg)	Ambient temperature (°C)	Microwave power (kW)	Maximum draw ratio	Strain rate (min^{-1})	Sonic modulus (GPa)
1	$21._5$	130	0.3	28	0.4_5	48
2	19	120	0.4	28	0.5_6	47
3	17	110	0.4	33	0.8	46
4	16	110	0.4	34	1.4	43

Mechanical properties

Drawn samples with different draw ratios were prepared at the optimum tensile loads and ambient temperatures listed in *Table 2* by controlling the microwave power. *Figure 9* shows the dependence of dynamic modulus E' on λ for different grade samples; λ is based upon the ratio of the precursor and product cross-sectional areas. The cross-sectional area was determined by weighing a sample of length 10 cm, which was used for dynamic modulus measurements, and using a constant density of 1.42 g cm^{-3}. These λ values were close to the ratios of take-up speed to feed speed. While the density of drawn samples excluding voids may range from 1.42 g cm^{-3} to 1.491 g cm^{-3} (crystalline density), the density difference is only 5%. Therefore, the value of E' calculated from a constant value of 1.42 g cm^{-3} is considered to be almost that for a drawn sample without voids. At a given λ a higher modulus is obtained for higher $\bar{M}_n$ samples. The highest dynamic modulus of ~54 GPa was obtained for three higher $\bar{M}_n$ samples. For sample 4, with the lowest $\bar{M}_n$, the attainable dynamic modulus was 51 GPa. The dynamic moduli are about 6 to 8 GPa higher than the sonic moduli listed in *Table 2*. This discrepancy is mainly due to the time dependence of the modulus. As an example, the time dependence of sonic modulus for a drawn sample is shown in *Figure 10*. The sonic modulus increased with time after drawing and levelled off above more than half a day. For this interval the sonic modulus changed from 38 GPa to 43 GPa. In this work the sonic modulus was measured immediately after drawing, while the dynamic modulus was measured several days later. Another reason for the discrepancy is that the sonic modulus may be underestimated owing to the occurrence of voids.

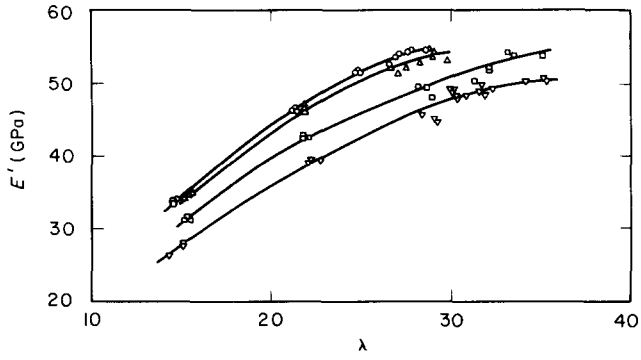

Figure 9 Variation of dynamic modulus, E', with draw ratio, λ. ○, sample 1; △, sample 2; □, sample 3; ▽, sample 4

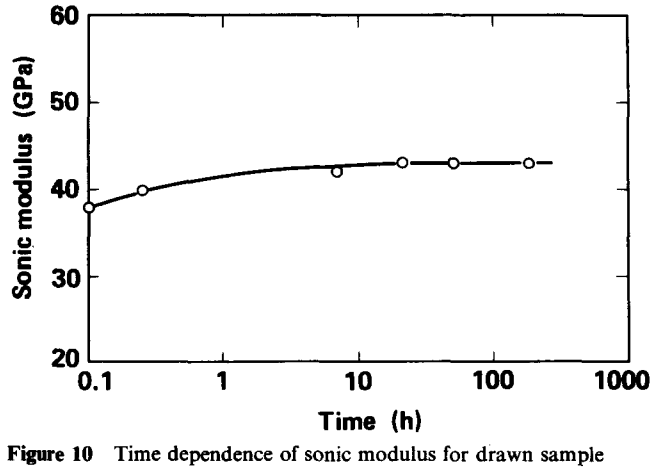

Figure 10 Time dependence of sonic modulus for drawn sample

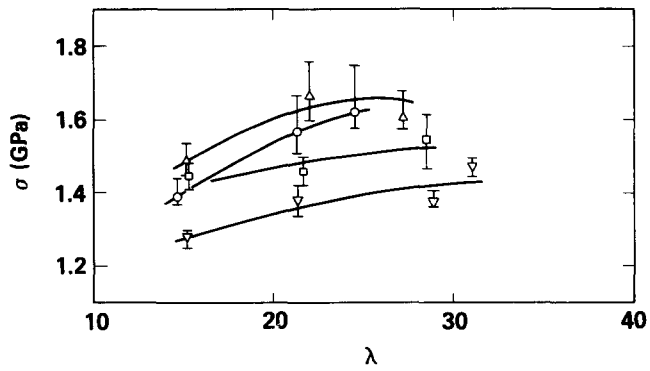

Figure 11 Variation of tensile strength, σ, with draw ratio, λ. ○, sample 1; △, sample 2; □, sample 3; ▽, sample 4

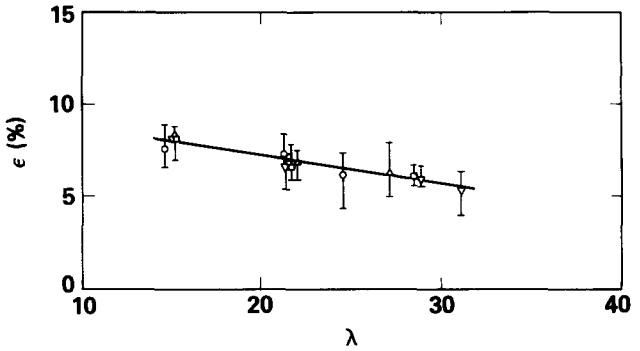

Figure 12 Variation of elongation at break, ε, with draw ratio, λ. ○, sample 1; △, sample 2; □, sample 3; ▽, sample 4

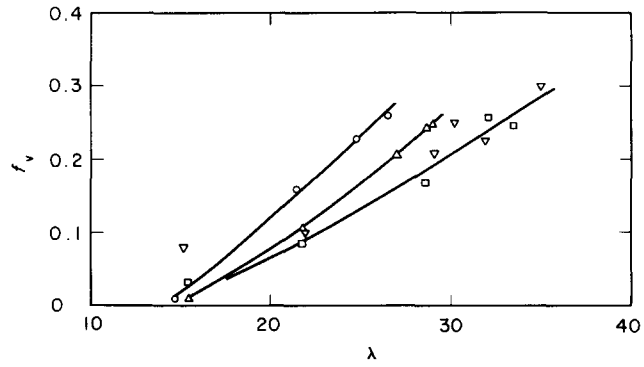

Figure 13 Dependence of void fraction, f_v, on draw ratio, λ. ○, sample 1; △, sample 2; □, sample 3; ▽, sample 4

Figure 11 shows the dependence of tensile strength σ on λ. Higher strengths are obtained for samples with higher $\bar{M}_n$. The dependence of elongation at break, ε, on λ is shown in *Figure 12*. The elongation decreases from 8 to 5% as λ increases from 15 to 30. There is no difference among samples 1 to 4.

For highly drawn samples internal voids are formed; the void fraction increases with increasing draw ratio[4,9]. *Figure 13* shows the dependence of void fraction on λ for different samples. The void fraction at the same λ is higher for higher $\bar{M}_n$ samples, which occurs because the samples of higher $\bar{M}_n$ were drawn under higher tensile loads. For example, sample 1 was drawn at a tensile load of 21.$_5$ kg, while sample 4 was drawn at 16 kg. The formation of such internal voids reduces the apparent dynamic modulus (E'_{app}) and tensile strength (σ_{app}) which are defined as follows.

$$E'_{app} = E'(1 - f_v) \quad (9)$$

$$\sigma_{app} = \sigma(1 - f_v) \quad (10)$$

Figures 14 and *15* show plots of E'_{app}–λ and σ_{app}–λ, respectively. Although the dynamic modulus and tensile strength of drawn POM itself increase with λ, as seen in *Figures 9* and *11*, E'_{app} shows an almost constant value of ~40 GPa for $\lambda > 20$ for three samples with higher $\bar{M}_n$, and σ_{app} decreases with λ because the void fraction increases with λ. The highest tensile modulus is obtained for three samples with higher $\bar{M}_n$, i.e. samples 1 to 3, as seen in *Figures 9* and *14*, while the highest tensile strength is obtained for sample 2 with $\bar{M}_n$ of 63 000 as seen in *Figures 11* and *15*.

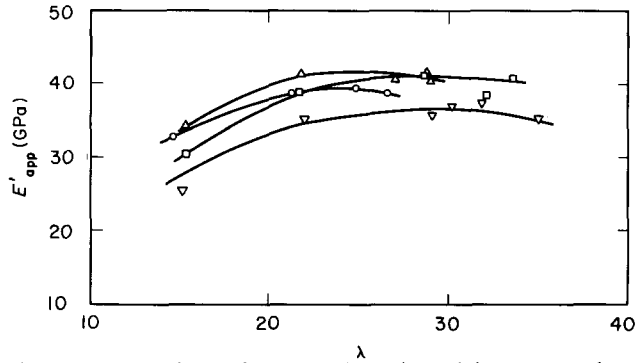

Figure 14 Dependence of apparent dynamic modulus, E'_{app}, on draw ratio, λ. ○, sample 1; △, sample 2; □, sample 3; ▽, sample 4

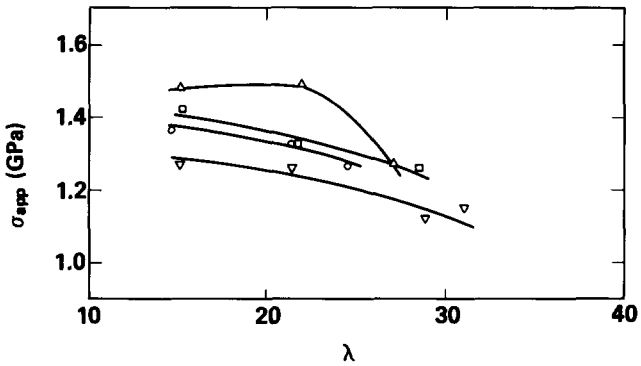

Figure 15 Dependence of apparent tensile strength, σ_{app}, on draw ratio, λ. ○, sample 1; △, sample 2; □, sample 3; ▽, sample 4

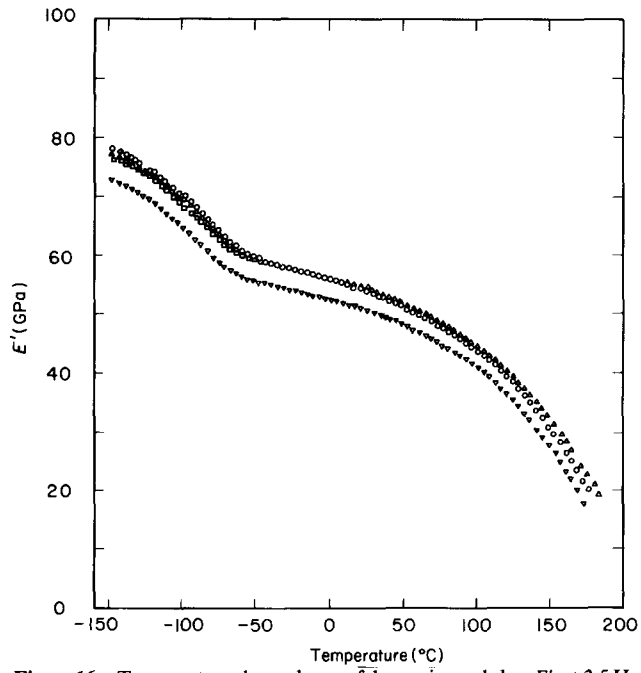

Figure 16 Temperature dependence of dynamic modulus, E', at 3.5 Hz. ○, sample 1, $\lambda = 28$; △, sample 2, $\lambda = 28$; □, sample 3, $\lambda = 33$; ▽, sample 4, $\lambda = 34$

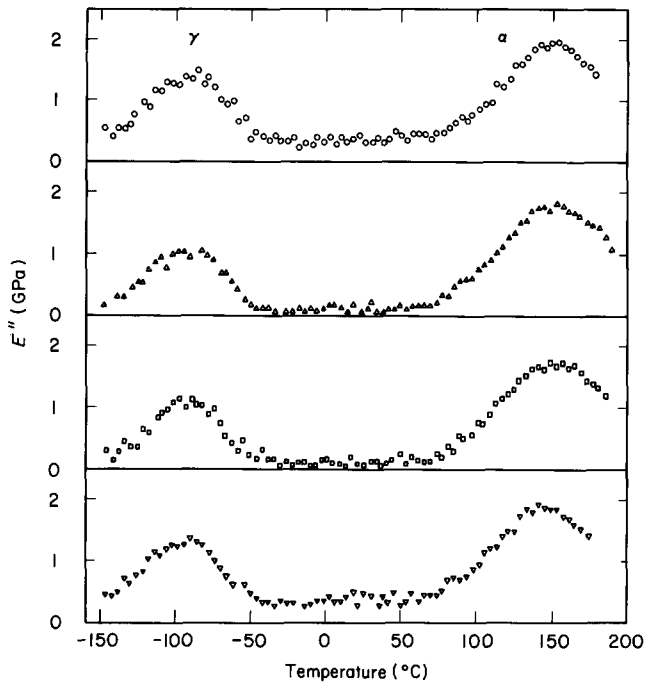

Figure 17 Temperature dependence of loss modulus, E'', at 3.5 Hz. ○, sample 1, $\lambda = 28$; △, sample 2, $\lambda = 28$; □, sample 3, $\lambda = 33$; ▽, sample 4, $\lambda = 34$

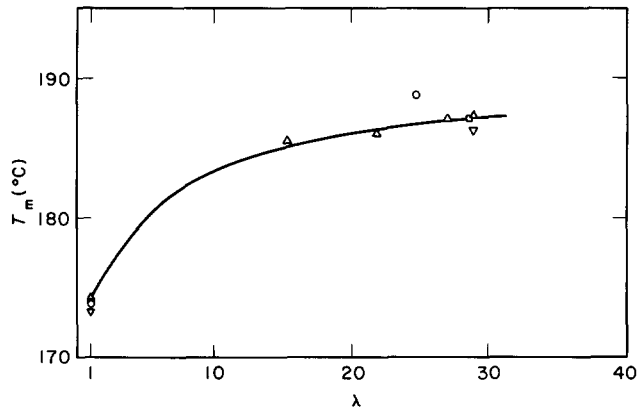

Figure 18 Dependence of melting temperature, T_m, on draw ratio, λ; heating rate 10 K min^{-1}, sample weight 5 mg. ○, sample 1; △, sample 2; □, sample 3; ▽, sample 4

Figures 16 and *17* show the temperature dependence of dynamic modulus (storage modulus) and loss modulus, respectively, at 3.5 Hz for samples 1–4 with the attainable λ. Similar properties were obtained for three samples with higher $\bar{M}_n$. Although the optimum strain rate for drawing under microwave heating decreases from 0.8 to 0.4_5 min^{-1} with increasing $\bar{M}_n$ from 47 000 to 66 000 (sample 3 to sample 1), as given in *Table 2*, it was not clearly observed that the α and/or γ relaxation temperatures shift to higher temperatures with $\bar{M}_n$. The dynamic modulus of sample 4 with the lowest $\bar{M}_n$ is ~5 GPa lower than that of the other three samples over the measured temperature range. The α relaxation temperature for sample 4 is about 10°C lower than that for the other three samples. This means that the molecular chains in crystalline regions in sample 4 are more mobile and can be rearranged at the highest strain rate of 1.4 min^{-1} under microwave heat-drawing.

Melting behaviour

Figures 18 and *19* show the dependence of melting temperature and heat of fusion, respectively, on λ for

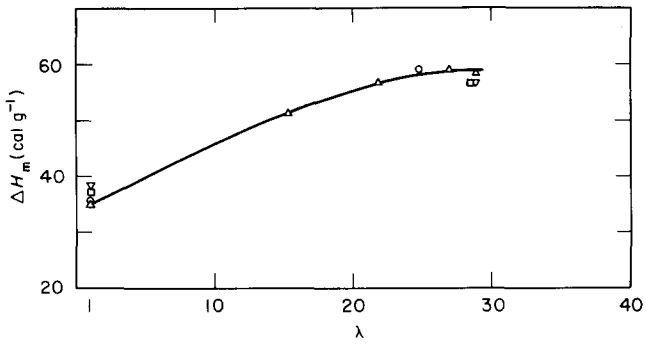

Figure 19 Dependence of heat of fusion, ΔH_m, on draw ratio, λ; heating rate 10 K min^{-1}, sample weight 5 mg. ○, sample 1; △, sample 2; □, sample 3; ▽, sample 4

samples 1–4 prepared under optimum drawing conditions. High melting temperature and high heat of fusion are obtained regardless of the molecular weight by preparing the drawn materials under the optimum conditions.

CONCLUSION

The drawing behaviour of POM under microwave heating depends on molecular weight. The highest draw ratio and the highest tensile modulus are obtainable by specifying the tensile load, ambient temperature, ambient temperature gradient and strain rate. The optimum tensile load and ambient temperature for high modulus increase with the molecular weight, while the optimum strain rate decreases. Although the attainable draw ratio decreases with the molecular weight, the highest tensile modulus (54 GPa) and strength (1.6 GPa) are obtained for samples with $\bar{M}_n > 47\,000$. In the conventional drawing method the optimum grade for high draw and high modulus was stated to be Delrin 500 grade ($\bar{M}_n = 45\,000$)[7]. In the microwave heat-drawing method the highest tensile modulus is obtainable even for the sample with the highest $\bar{M}_n$ of 66 000. Within the range examined, the optimum $\bar{M}_n$ for high modulus and high strength is 63 000 (sample 2), since the internal voids increase with the molecular weight.

REFERENCES

1 Nakagawa, K., Maeda, O. and Yamakawa, S. *J. Polym. Sci., Polym. Lett. Edn.* 1983, **21**, 933
2 Takeuchi, Y., Yamamoto, F. and Nakagawa, K. *J. Polym. Sci., Polym. Lett. Edn.* 1984, **22**, 159
3 Nakagawa, K., Konaka, T. and Yamakawa, S. *Polymer* 1985, **26**, 84
4 Konaka, T., Nakagawa, K. and Yamakawa, S. *Polymer* 1985, **26**, 462
5 Takeuchi, Y., Yamamoto, F., Nakagawa, K. and Yamakawa, S. *J. Polym. Sci., Polym. Phys. Edn.* 1985, **23**, 1193
6 Ciferri, A. and Ward, I. M. 'Ultra-High Modulus Polymers', Applied Science, London, 1979
7 Brew, B. and Ward, I. M. *Polymer* 1978, **19**, 1338
8 Nakagawa, K. and Konaka, T. *Polymer* 1986, **27**, 1031–1036
9 Jarecki, L. and Meier, D. J. *J. Polym. Sci., Polym. Phys. Edn.* 1979, **17**, 1611